NJC

ROYAL SOCIETY OF CHEMISTRY

PAPER

View Article Online
View Journal

Cite this: DOI: 10.1039/d5nj01780g

In situ preparation of a recyclable hydrogel-based photocatalyst and its application in sunlight-promoted photodegradation of eosin Y

Xiaoxia Liu,[a] Sa Yang,[a] Yanli Cheng,[a] Donglei Wei, *[ac] Hou Chen, *[bc] Liangjiu Bai,[bc] Wenxiang Wang,[bc] Huawei Yang,[ac] Lixia Yang[b] and Kun Yin[a]

Received 25th April 2025,
Accepted 28th July 2025

DOI: 10.1039/d5nj01780g

rsc.li/njc

A hydrogel-based photocatalyst is synthesized by the construction of a hydrogel skeleton using common monomers and subsequent *in situ* generation of Zn–Cu–S photocatalyst particles. The photocatalytic degradation performance of the hydrogel-based photocatalyst is systematically studied, and the photocatalyst exhibits good removal ability for eosin Y. The composite photocatalyst shows high efficiency at low loading, with a removal rate of up to >98% in 3 hours under sunlight irradiation, without the need for a preliminary dark adsorption process. High removal efficiency was observed, remaining above 95% even after 10 recycling runs, demonstrating the excellent stability of the composite photocatalyst. We thus provide a facile method to construct hydrogel-based photocatalysts that show high application potential in the photocatalytic removal of eosin Y.

1. Introduction

The efficient removal of organic dyes from wastewater has attracted great attention because these dyes are usually highly diversified, water-soluble and resistant to biodegradation, causing environmental pollution and health problems.[1,2] Eosin Y is one of the most widely used organic dyes that is commonly used in the painting, rubber, dyestuff and textile industries.[3,4] The accumulation of eosin Y in the human body brings health problems such as blurred vision, respiratory paralysis, and heart disease.[5] Adsorption,[6] membrane ultrafiltration,[7] biological treatment,[8] ion exchange,[9] advanced oxidation,[10] and other methods[11] are commonly used for the removal of organic dyes from aqueous media. Advanced oxidation technologies, such as electrochemical catalytic oxidation,[12] ultrasonic oxidation,[13] and Fenton oxidation,[14] can completely break down the structure of dye molecules without forming harmful secondary products.[15] The development of photo-Fenton techniques using light energy for the removal of organic dyes has extended the application of the oxidation technique.[16–19] Photocatalysis has attracted much attention in recent years due to its advantages of green energy utilization, high catalytic performance, easy operation, and low-toxicity or non-toxic degradation products.[20,21] A variety of photocatalysts, such as metal oxides, metal sulfides, and inorganic semiconductors, have been used to catalyze the degradation of eosin Y.[22–24] Among them, copper-doped zinc sulfide semiconductors (namely, zinc copper sulfide, Zn–Cu–S) are the commonly used, inexpensive, non-toxic photocatalysts that exhibit good thermal stability, high absorption in the visible region, and excellent electron transport properties as well as are capable of rapid electron–hole pair generation. They exhibit high efficiency and wide applicability in dye-containing wastewater treatment.[25–28] Despite these exciting reports, challenges remain that require further investigation. In previous studies, most of the Zn–Cu–S photocatalysts were prepared using solvothermal methods and obtained as nano- or micron-sized particles.[29] In most works, the efficient removal of organic dyes usually required a large amount of catalysts, and significant loss of the catalysts and catalytic efficiency was observed during recycling experiments because the small size of the catalysts complicated the recovery step.[30,31]

Many attempts have been made to achieve low catalyst loading and easy recovery. The loading of photocatalyst particles onto two-dimensional substrates, such as fiberglass and Ti mesh, has been reported and showed good removal ability.[32–35] Most of the substrates used in these works were opaque, with light absorption occurring only on one side of the material.[36] A hydrogel is a highly hydrophilic organic material composed of a three-dimensional cross-linked network. It has been widely used in many fields, such as tissue engineering, pollutant

[a] School of Chemistry and Chemical Engineering, Ludong University, Yantai, Shandong, 264025, China. E-mail: weidonglei@ldu.edu.cn
[b] School of Materials Science and Engineering, Ludong University, Yantai, Shandong, 264025, China. E-mail: chenhou@ldu.edu.cn
[c] Shandong Key Laboratory of Carbon Fiber and Composite Materials Manufacture and Application, Weihai, Shandong, 264211, China

detection, and flexible wearable electronic devices,[37–39] and offers the advantages of easy preparation, large specific surface area, high light transmittance and easy recyclability.[40,41] The excellent mass transfer channels in hydrogel make it a good carrier for photocatalysts. Moreover, loading the photocatalyst into the hydrogel brings additional advantages such as uniform distribution, reduced agglomeration, and lowered electron–hole complexation of the photocatalyst.[42,43] Several works have examined the loading of photocatalysts into hydrogels for the treatment of dye-containing water. These include loading the already-prepared photocatalyst particles into the channels of the hydrogels,[44–48] or simply through *in situ* preparation of the photocatalyst directly in the channels of the hydrogels.[49–51] Hydrothermal synthesis represents a powerful method for the photocatalyst preparation steps; however, the skeleton of the hydrogel must be designed to tolerate the high temperatures. Thus, an alternative method of precipitation that occurs directly in the channels of the hydrogel may overcome this restriction and provide a more straightforward way to prepare the hydrogel-based photocatalyst. To reduce the catalyst loading without decreasing the catalytic efficiency, and widen the applicability of the hydrogel-based photocatalyst with a simple catalyst preparation process, herein, the hydrogel-based photocatalyst was prepared *via in situ* precipitation of Zn–Cu–S particles in the channels of the hydrogel. The recyclable photocatalyst showed good catalytic performance for the removal of eosin Y from aqueous media.

2. Experimental section

2.1. Materials

Acrylamide (AM) was purchased from Macklin Biotechnology Co., Ltd. 2-Hydroxyethyl methacrylate (HEMA) and $Na_2S{\cdot}9H_2O$ were purchased from Energy Chemical Co., Ltd. *N*,*N*′-Methylenebisacrylamide (BIS), *N*,*N*,*N*′,*N*′-tetramethyl ethylenediamine (TMEDA), potassium persulfate (KPS), eosin Y, and $Zn(NO_3)_2{\cdot}6H_2O$ were purchased from Sinopharm Chemical Reagents Co., Ltd. $Cu(NO_3)_2{\cdot}3H_2O$ was purchased from Shanghai Aladdin Biochemical Technology Co., Ltd. HEMA was treated by passing through neutral alumina before use. Other regents and solvents were purchased from commercial sources and used as received. Deionized water was obtained from a UPH-I-40 L superpurification system.

2.2. Instrumentations

The concentration of eosin Y was determined by UV-Vis absorption analysis. The UV-Vis absorption spectra of eosin Y were recorded in a 1 cm path quartz cuvette on a SHIMADZU UV-2550 UV-Visible spectrophotometer. The UV-Visible diffuse reflectance absorption spectra of the hydrogel-based photocatalysts were recorded using a UV-Visible near-infrared spectrophotometer (UV-3600; Shimadzu, Japan). The morphology of the hydrogel-based photocatalyst was observed using a scanning electron microscope (SEM, Hitachi SU-8010). The presence of certain functional groups in the catalysts was determined using Fourier transform infrared spectroscopy (FT-IR, Nicolet iS50) in the wavelength range of 400–4000 cm^{-1}. The elements contained in the catalysts were determined using X-ray photoelectron spectroscopy (XPS, ESCALAB Xi+) in the low-resolution scanning range of 0–4000 eV and high-resolution scanning range of N 1s, O 1s, C 1s, Zn 2p, Cu 2p and S 2p orbitals. The crystal type of the hydrogel-based photocatalyst was determined using X-ray diffraction (XRD, Bruker D8) with a diffraction angle 2θ in the range of 5°–80°. The hydrogel-based photocatalyst was analyzed for reactive oxygen species (ROS) produced under light irradiation using electron spin resonance (ESR, Bruker, Germany, A300-10/12). The concentrations of the remaining Zn(II) and Cu(II) in the mixed Zn(II)–Cu(II) solution after adsorption by the hydrogel were measured using an atomic absorption spectrophotometer (AAS, AA240).

2.3. Synthesis of hydrogel-based photocatalyst

With Gel@ZnCuS-3 as an example. AM (2.14 g, 30 mmol, 100 equiv.), HEMA (0.375 mL, 3 mmol, 10 equiv.), BIS (0.093 g, 0.3 mmol, 1 equiv.), KPS (12.2 mg, 0.045 mmol, 0.15 equiv.), and TMEDA (37.5 μL, 0.3 mmol, 1 equiv.) were added to water (15 mL). The mixture was evenly divided into 30 parts, placed in a mold, and heated in a water bath at 65 °C for 20 min to form a cube of 1 × 1 × 0.5 cm. The prepared hydrogels were immersed and washed with H_2O, and the water was exchanged every 8 h for 3 times. Hydrogels with different ratios of n(AM) : n(BIS) = 60 : 1, 80 : 1, 120 : 1 were prepared according to the above procedure (Table 1).

The prepared hydrogels were placed in 100 mL of a mixed solution containing 20 mmol L^{-1} $Zn(NO_3)_2$ and 2 mmol L^{-1} $Cu(NO_3)_2$, and shaken for 4 h. The hydrogel was then placed in 100 mL of a solution containing 20 mmol L^{-1} Na_2S and shaken for 2 h to obtain the hydrogel-based photocatalyst. The hydrogel-based photocatalyst was washed with water for 48 h (with water exchange every 12 h) to remove the unreacted ions. The prepared hydrogel-based photocatalyst was kept in deoxygenated water. Atomic absorption was used to determine the concentration of Zn(II) and Cu(II) in the solution after adsorption to obtain the loading ratios of Zn(II) and Cu(II) in the hydrogel-based photocatalyst.

The concentration of the remaining Zn(II) and Cu(II) in the mixed Zn(II)-Cu(II) solution after adsorption by the hydrogel was measured using AAS analysis. These two metal ions were not detected in the cleaning solution of the hydrogel-based photocatalyst. Thus, the catalyst loading and the ratio of n(Zn) : n(Cu)

Table 1 Preparation of hydrogel-based photocatalysts

Photocatalyst	n(Zn) : n(Cu)	n(AM) : n(HEMA)
Gel@ZnCuS-1	90 : 10	60 : 1
Gel@ZnCuS-2	90 : 10	80 : 1
Gel@ZnCuS-3	90 : 10	100 : 1
Gel@ZnCuS-4	90 : 10	120 : 1
Gel@ZnCuS-5	85 : 15	100 : 1
Gel@ZnCuS-6	95 : 5	100 : 1
Gel@ZnCuS-7	98 : 2	100 : 1

in the prepared photocatalyst were calculated according to the concentration change of the solution.

Hydrogel-based photocatalysts were prepared using solutions with different Zn(II) and Cu(II) concentrations (n(Zn) : n(Cu) = 98 : 2, 95 : 5, 85 : 15) by using the same procedure (Table 1).

2.4. General procedure for the photodegradation of eosin Y by the hydrogel-based photocatalyst

The hydrogel-based photocatalyst was added to 10 mL of 100 mg L^{-1} eosin Y and photodegraded under a light source for 3 h. When the reaction was complete, 2 mL of the solution was taken and used to determine the concentration. Parallel experiments were conducted for the photocatalytic degradation experiments.

The removal rate of eosin Y was calculated from the following equation:

$$R(\%) = (C_0 - C)/C_0 \quad (1)$$

where C is the remaining concentration of eosin Y (mg L^{-1}) and C_0 is the initial concentration of eosin Y (mg L^{-1}).

2.5. Photocatalytic kinetic study

The hydrogel-based photocatalyst was added to 10 mL of 100 mg L^{-1} eosin Y and illuminated with sunlight for 3 h. A solution of 2 μL was extracted and diluted to 2 mL every 20 min to determine the concentration of eosin Y.

The K_{app} was calculated from the following equation:

$$\ln(C_0/C_t) = K_{app}t \quad (2)$$

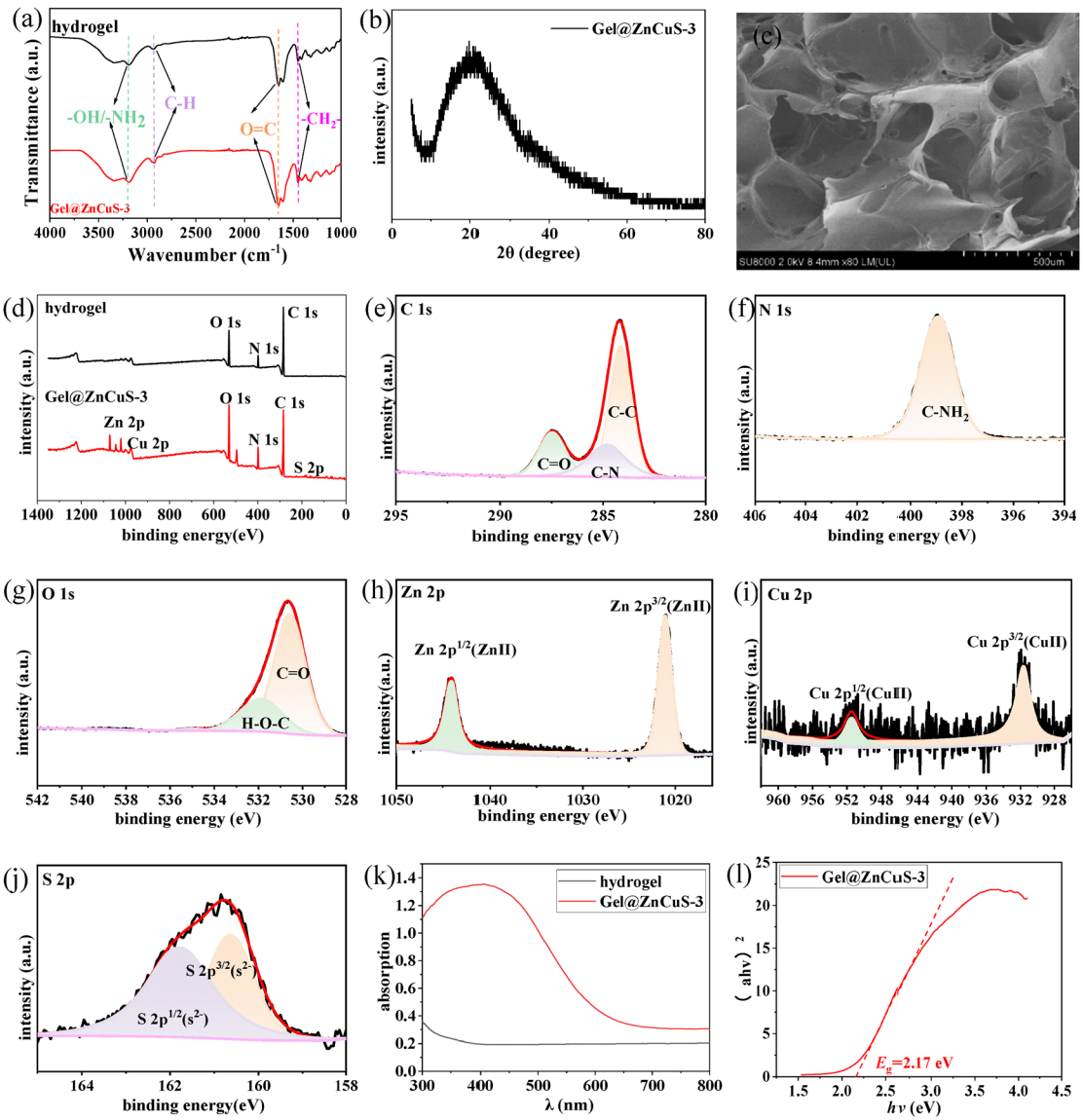

Fig. 1 (a) FT-IR spectra of the hydrogel before and after loading of Zn–Cu–S, (b) XRD patterns and (c) SEM image of Gel@ZnCuS-3, (d) XPS wide scan of the hydrogel before and after loading of Zn–Cu–S, (e) C 1s, (f) N 1s, (g) O 1s, (h) Zn 2p, (i) Cu 2p and (j) S 2p, (k) UV-vis diffuse reflectance spectroscopy, (l) $(\alpha h\nu)^2$ *vs.* $h\nu$ plot for Gel@ZnCuS-3.

where C_0 and C_t are the concentrations of eosin Y at the initial time and time t, respectively.

2.6. Reusability of the hydrogel-based photocatalyst

The hydrogel-based photocatalyst was added to 10 mL of 100 mg L^{-1} eosin Y and illuminated under sunlight for 3 h. When the reaction was complete, 2 mL of the solution was taken and used to determine the concentration of eosin Y. The hydrogel-based photocatalyst was washed in water for 24 h. The photocatalytic experiment was carried out using the washed hydrogel-based photocatalyst under the same conditions. The recycling experiments were repeated 10 times, and the concentration of eosin Y after each degradation process was recorded.

3. Results and discussion

3.1. Characterization

Fourier transform infrared spectroscopy (FT-IR) analysis was used to analyze the structure of the hydrogel-based photocatalyst. The FT-IR spectra of the hydrogels before and after loading of Zn–Cu–S (Gel@ZnCuS-3 as an example) are shown in Fig. 1a. The peaks in the region of 3200–3600 cm^{-1} are attributed to the stretching vibration of the O–H and N–H bonds. The peaks at 3000–2835 cm^{-1} are related to the stretch vibration of C–H bonds. The spectra also show signals typical of both co-monomers, as the carbonyl bands from amides and esters, at approximately 1660 and 1715 cm^{-1}, respectively.[52] The spectra exhibit similar characteristic peaks for these two materials, which may be attributed to the low loading of the Zn–Cu–S and the fact that no new bonds were formed during the catalyst loading process. The crystallinity of the lyophilized hydrogel was analyzed by XRD (Fig. 1b). Bragg reflections showed a broad peak at $2\theta = 22.5^\circ$, confirming the amorphous nature of the hydrogel. No crystal-derived peak was observed in the spectrum, indicating that there was no unreacted monomer residue in the hydrogel.[53] The XRD spectrum of Zn–Cu–S was reported to show strong diffraction peaks at $2\theta = 28.8^\circ$ and 47.8°,[54] but the characteristic diffraction peaks were not clearly observed in our study due to the overlap of the signal with that of the hydrogel. The XRD spectra of other hydrogel-based photocatalysts, shown in Fig. S2, were similar to that of Gel@ZnCuS-3. The cross-section morphology of the hydrogel-based photocatalyst Gel@ZnCuS-3 was characterized by scanning electron microscopy (SEM). As shown in Fig. 1c, the image reveals that the hydrogel has a three-dimensional mesh structure with irregularly shaped micropores and interconnected channels. This may provide large numbers of active sites for catalyst loading in the hydrogel and facilitate extensive contact between the catalyst and the contaminants during the adsorption/photocatalysis process.[55] EDS-mapping was used to characterize Gel@ZnCuS-3 and, as shown in Fig. S3, the images reveal that the Zn–Cu–S particles are uniformly distributed in the hydrogel matrix.

The surface elemental and chemical bonding compositions of the hydrogel and Gel@ZnCuS-3 were further investigated using X-ray photoelectron spectroscopy (XPS) analysis. The low-resolution XPS spectrum of the hydrogel confirmed the presence of C, N and O elements. New peaks at 1021, 951 and 161 eV, attributed to Zn, Cu and S elements, are also seen in the low-resolution XPS spectra of Gel@ZnCuS-3, which are introduced during the catalyst loading process (Fig. 1d). The results of the high-resolution C 1s, N 1s, O 1s, Zn 2p, Cu 2p and S 2p XPS spectra of Gel@ZnCuS-3 also confirmed the structure of the synthesized composite photocatalyst (Fig. 1e–j). In the C 1s spectrum, the peak can be divided into C–C, C═C and C–N bonds, with binding energies of 284.8, 287.5 and 284.9 eV. In the N 1s spectrum, the peak at 398.95 eV is attributed to the C–N bond. The O 1s peak is divided into C═O and O–H bonds at binding energies of 530.6 and 530.0 eV. The characteristic peaks of Zn (Zn $2p^{3/2}$ at 1043.9 eV and Zn $2p^{1/2}$ at 1021.1 eV) and Cu (Cu $2p^{1/2}$ at 951.7 eV and Cu $2p^{3/2}$ at 931.6 eV) are also consistent with the bivalent state of these elements.[56] The peaks at 161.8 eV (attributed to S $2p^{1/2}$) and 160.7 eV (attributed to S $2p^{3/2}$) indicate the presence of divalent-state S.

The changes in the optical properties of hydrogels before and after loading of Zn–Cu–S photocatalyst were investigated by UV-Vis diffuse reflectance spectroscopy (Fig. 1k). The absorption intensity of Gel@ZnCuS-3 was enhanced in the region of $\lambda > 400$ nm, indicating the enhanced visible light absorption ability of the hydrogel-based photocatalyst. The absorption intensity of the hydrogel remained nearly constant without clear absorption peaks in the visible region. Based on these results, the band gap energy (E_g) of the photocatalyst Gel@ZnCuS-3 was characterized using the hydrogel-based photocatalyst by ignoring the influence of the hydrogel substrate, and calculated to be 2.17 eV by the Kubelka–Munk equation (Fig. 1l). The conduction band potential (CB) and valence band potential (VB) of Gel@ZnCuS-3 are calculated to be −0.33 eV and 1.84 eV, respectively (for calculation details, see the SI). On the basis of the above characterization results, and given that, to our knowledge, no related reports indicate that any covalent bonds are formed during the precipitation process, the Zn–Cu–S particles are expected to form in the channels of the hydrogel *via* physical deposition.

3.2. Photocatalytic degradation of eosin Y

The prepared hydrogel-based photocatalysts were exposed to sunlight to investigate their performance in the photocatalytic degradation of eosin Y. The hydrogel-based photocatalysts with different ratios of monomer and cross-linking reagents ranging from 60 : 1 to 120 : 1 were tested with (gray) and without (green) a 1-hour dark period (Fig. 2a). The photocatalytic degradation ability of the hydrogel-based photocatalyst on eosin Y slightly increased with an increasing ratio of the monomer to cross-linking reagent. An eosin Y removal rate of 98.4% was achieved with the hydrogel-based photocatalyst Gel@ZnCuS-3, with a monomer to cross-linking reagent ratio of 100 : 1. The hydrogel-based photocatalyst became swollen and friable when the monomer and cross-linking reagent ratio was increased to 120 : 1, which may be due to incomplete cross-linking of the hydrogel, leading to a decreased removal rate (93%). The

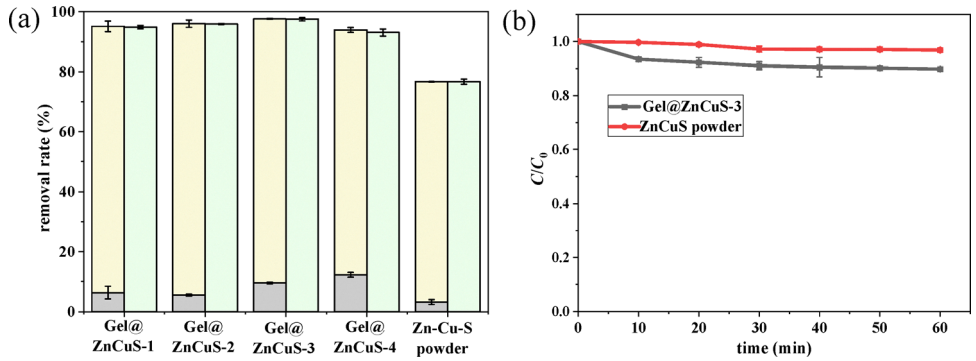

Fig. 2 (a) Influence of the dark reaction on the removal of eosin Y by hydrogel-based photocatalysts (C_0, 100 ppm), dark reaction for 1 h (gray), followed by sunlight irradiation for 3 h (yellow), and reaction directly irradiated by sunlight for 3 h (green); (b) removal of eosin Y by Gel@ZnCuS-3 and Cu–Zn–S powder under dark conditions (t, 3 h; C_0, 100 ppm).

photodegradation performance of the hydrothermally synthesized Zn–Cu–S particles upon removal of eosin Y was also tested as a comparison to the hydrogel-based photocatalyst. Lower removal rate (76.7%) was observed even when a larger amount of photocatalyst was used (100 mg), demonstrating that the strategy of loading the photocatalyst into the hydrogel can accelerate the photodegradation process.[57] Holding the reaction mixture in the dark before exposure to sunlight seemed to have little influence on the removal of eosin Y. Detailed adsorption kinetics assays under dark conditions were performed for the hydrogel-based photocatalyst and Zn–Cu–S particles as a comparison to achieve further insight into the influence of dark reactions on the removal of eosin Y (Fig. 2b). The equilibrium of adsorption and desorption was reached in approximately 30 min for both the hydrogel-based photocatalyst and Zn–Cu–S particles. The adsorption of eosin Y by the hydrogel-based photocatalyst was only approximately 10%, indicating that photodegradation is the main process for the removal of eosin Y. The low adsorption efficiency of Gel@ZnCuS-3 on eosin Y under dark conditions may be attributed to the abundant acylamino and hydroxyl functional groups in the hydrogel, which may induce electrical repulsion of the eosin Y anion. On the basis of these results, subsequent photodegradation experiments were conducted under direct irradiation with sunlight without a dark period for adsorption equilibrium.

The photocatalytic performance of the hydrogel-based photocatalysts obtained by immersing the hydrogel into solutions containing different ratios of Zn(II) and Cu(II) was investigated; the results are listed in Fig. 3. The highest removal rate was observed when a ratio of Zn(II) to Cu(II) of 9 : 1 (Gel@ZnCuS-3) was used as the immersion solution. The removal rate decreased with either an increase or a decrease in the ratio of Zn(II) to Cu(II).

Bench experiments for the photodegradation of eosin Y by Gel@ZnCuS-3 were conducted in various solution concentrations (20–100 mg L^{-1}) to test the removal ability of the hydrogel-based photocatalyst (Fig. 4a). The results showed that the removal rate increased at lower concentrations of eosin Y, and reached >99% at a concentration of 20 mg L^{-1} under irradiation with sunlight. When other light sources, such as

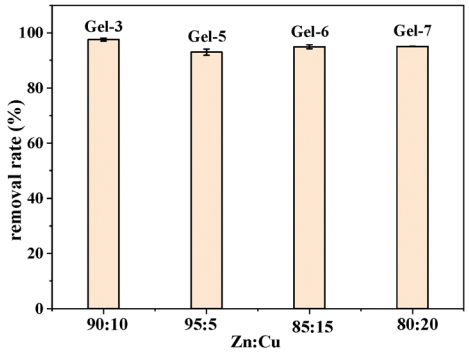

Fig. 3 Effect of Zn(II)/Cu(II) solution concentration on eosin Y removal (sunlight, t, 3 h; C_0, 100 ppm).

mercury lamp (green), white LEDs (purple), and blue LEDs (blue), were used, the removal rate showed an apparent decrease, which may be attributed to the low light intensity of these light sources (see the SI for light intensity data). It is worth noting that even with a low catalyst loading of the Zn–Cu–S photocatalyst and under mild reaction conditions, a practical removal rate of 84.5% was observed when using white LEDs. The photodegradation of eosin Y by Gel@ZnCuS-3 in different solution volumes (5–20 mL) and constant solution concentration (100 mg L^{-1}) was conducted; the results are shown in Fig. 4b. Due to the excess of eosin Y in the solution, the removal rate decreased with increasing solution volume. The results show the high application potential of the hydrogel-based photocatalyst for various conditions.

The photocatalytic activity of Gel@ZnCuS-3 for the degradation of eosin Y under solar irradiation was investigated. The photocatalyst showed enhanced removal performance with an increased removal rate under solar irradiation. Fig. 5a shows the kinetics results of eosin Y removal by Gel@ZnCuS-3 and Zn–Cu–S particles. To unravel the degradation mechanisms mediated by Gel@ZnCuS-3 and Zn–Cu–S powder, the degradation kinetic curve lines were simulated by fitting the kinetics to pseudo-first-order and pseudo-second-order models (Fig. 5b and c). A high correlation coefficient for the pseudo-first-order model for Zn–Cu–S particles (R^2 > 0.99) was

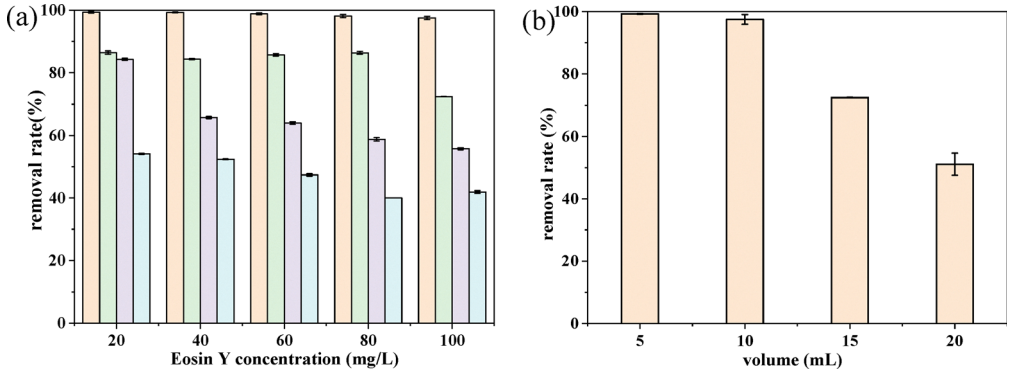

Fig. 4 (a) Influence of solution concentration on eosin Y removal by Gel@ZnCuS-3 under irradiation with sunlight (orange), UV light (green), white LEDs (purple) and blue LEDs (blue) (t, 3 h); (b) removal of eosin Y in different solution volumes by Gel@ZnCuS-3 (sunlight; t, 3 h; C_0, 100 ppm).

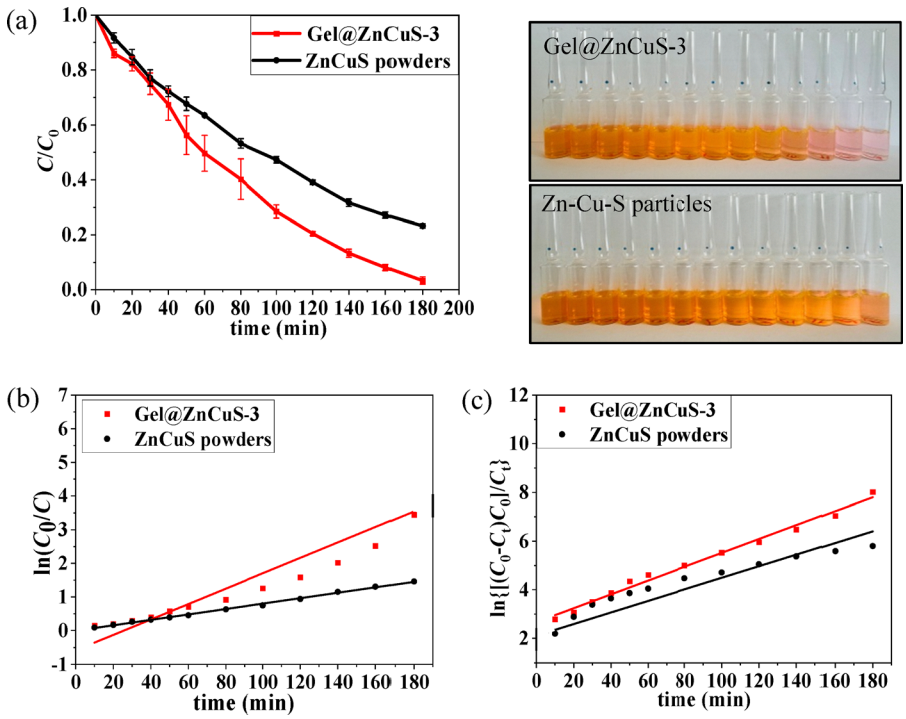

Fig. 5 (a) The photocatalytic degradation curves at different times; the inset shows photographs of the mixture at each time point (sunlight; t, 3 h; C_0, 100 ppm). (b) Pseudo-first-order and (c) the pseudo-second-order kinetic results.

observed. For Gel@ZnCuS-3, the correlation coefficient for the pseudo-first-order model was low ($R^2 < 0.4$), while the correlation coefficient for the pseudo-second-order model was high ($R^2 > 0.99$).[58–60]

It is well documented that pollutants are usually degraded by oxidizing substances, and that the main oxidizing species during photocatalytic oxidation are h^+, $^{\bullet}OH$ and $^{\bullet}O_2^-$. Scavenging of these oxidizing species reduces the photocatalytic efficiency, so their nature can be detected by adding different scavengers.[61,62] To characterize the species produced in the Gel@ZnCuS-3 system, benzoquinone (BQ), KI, and t-butanol (TBA) and were added as scavengers for the detection of h^+, $^{\bullet}OH$ and $^{\bullet}O_2^-$, respectively.[63] As shown in Fig. 6a, the photodegradation of eosin Y was significantly inhibited by the addition of BQ, and was slightly reduced in the presence of KI and TBA, indicating that h^+ and $^{\bullet}OH$ have limited roles in the degradation of eosin Y, whereas $^{\bullet}O_2^-$ has the major role. Electron spin resonance (ESR) characterization of $^{\bullet}O_2^-$ was performed for the Gel@ZnCuS-3 catalytic system under light irradiation, and the significant signal changes that were observed further confirmed the presence of $^{\bullet}O_2^-$ during the reaction (Fig. 6b). Based on the characterization and experimental results, a plausible photodegradation mechanism was proposed (Fig. 6c). Sunlight irradiation triggers the photocatalytic reaction, and the photogenerated electrons in the conduction band and photogenerated holes in the valence band are

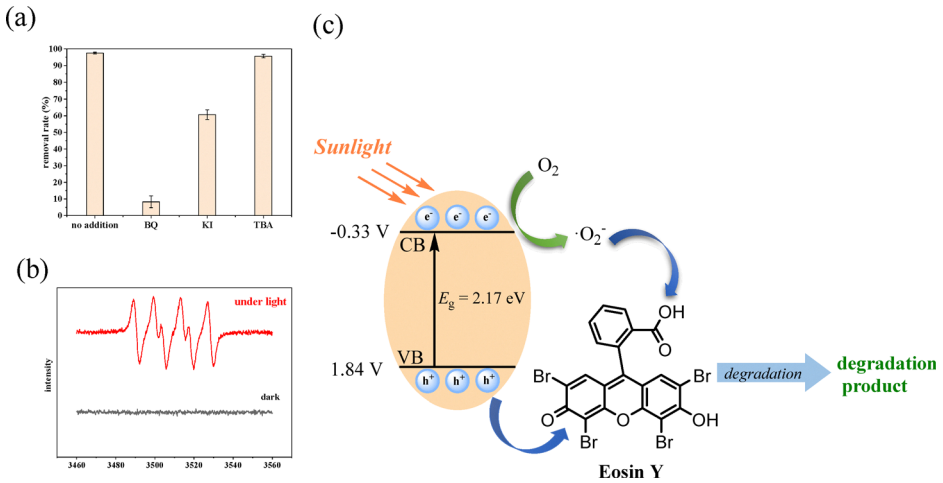

Fig. 6 (a) Effect of scavengers on photocatalysis (sunlight; *t*, 3 h; C_0, 100 ppm). (b) ESR spectra of Gel@ZnCuS-3 in water under irradiation with light and in the dark. (c) Proposed mechanism for the photodegradation of eosin Y by the hydrogel-based photocatalyst.

transferred to the photocatalyst's surface to initiate the redox reaction. The electron (e) reacts with O_2 to form a superoxide anion radical ($^{\bullet}O_2^-$), which can decompose the eosin Y molecule through a series of oxidizing and reducing reactions.[64] Direct decomposition of eosin Y may also occur at the holes of the photocatalyst.

The photocatalytic performances for the removal of eosin Y using the hydrogel-based photocatalyst prepared in this work and photocatalysts in the previous reports are listed in Table S1. Compared to the previous reports, in our work, the photocatalyst, which was obtained by a simple synthetic procedure, achieved high removal rates of eosin Y with low catalyst loading, and could be used in an increased number of recycling runs, demonstrating the stability of the hydrogel-based photocatalyst. Furthermore, the photocatalytic degradation performance of the hydrogel-based photocatalyst towards other organic contaminants was also examined (Fig. S4). It showed good photodegradation of methylene blue (removal rate of 98.5%) and acceptable removal rates of methyl orange (90.1%) and alizarin red (88.2%). When the hydrogel-based photocatalyst was used for the photodegradation of non-dyeing bisphenol A, a lower removal rate of 42% was observed.

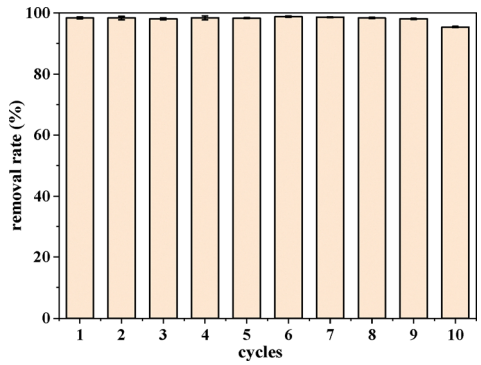

Fig. 7 Reusability of the hydrogel-based photocatalyst (sunlight; *t*, 3 h; C_0, 100 ppm).

An advantage of the hydrogel-based photocatalyst is that it can be easily separated from the reaction mixture after the photodegradation process. Recycling experiments were conducted to evaluate the reusability of the hydrogel-based photocatalyst (Fig. 7). The photocatalyst Gel@ZnCuS-3 retained high catalytic efficiency as the removal rate remained almost unchanged after 9 recycling runs (~98%). Only a slight decrease in removal rate (95.4%) was observed in the 10th recycling run. The recovery of the hydrogel-based photocatalyst is straightforward; simple soaking in water for approximately 12 hours under ambient conditions between recycling runs. When the reaction mixture in each cycle was analyzed by AAS to determine the leaching concentration, no metal ions were detected after the photodegradation process. These results demonstrate the high stability of the hydrogel-based photocatalyst and the high potential of this sunlight-promoted photocatalytic degradation strategy.

3. Conclusions

A facile synthesis of hydrogel-based photocatalysts was developed by constructing a hydrogel skeleton using common monomers and subsequent *in situ* generation of Zn–Cu–S photocatalyst particles in the channels of the hydrogel. The structure and optical properties of the hydrogel-based photocatalyst were confirmed by the characterization results. The composite photocatalyst was used in the photocatalytic degradation of eosin Y and exhibited high catalytic efficiency and good removal ability at low catalyst loading. The removal rate can reach approximately 98% in 3 hours under sunlight irradiation, without the need for a preliminary dark adsorption process. Moreover, the hydrogel-based photocatalyst showed excellent stability, with the removal efficiency maintained above 95% even after 10 recycling runs. This strategy provides a simple way to construct hydrogel-based photocatalysts and has high application potential for the photocatalytic removal of eosin Y.

Author contributions

Xiaoxia Liu: investigation, writing – original draft. Sa Yang: methodology. Yanli Cheng: formal analysis. Donglei Wei: writing – review & editing, project administration, funding acquisition. Hou Chen: conceptualization. Liangjiu Bai: funding acquisition. Wenxiang Wang: investigation. Huawei Yang: methodology. Lixia Yang: validation, supervision. Kun Yin: resources.

Conflicts of interest

The authors declare no conflicts of interest.

Data availability

The data that support the findings of this study are available from the corresponding author upon reasonable request.

Apparatus picture, calculation methods, catalytic performance comparison, and charicterization results. See DOI: https://doi.org/10.1039/d5nj01780g.

Acknowledgements

This work was financially supported by the Natural Science Foundation of Shandong Province (ZR2022MB114, ZR2023YQ043).

References

1 S. Bolisetty, M. Peydayesh and R. Mezzenga, Sustainable technologies for water purification from heavy metals: review and analysis, *Chem. Soc. Rev.*, 2019, **48**, 463–487.
2 E. Brillas and C. A. Martínez-Huitle, Decontamination of wastewaters containing synthetic organic dyes by electrochemical methods. An updated review, *Appl. Catal., B*, 2015, **166–167**, 603–643.
3 S. M. Derayea and D. M. Nagy, Application of a xanthene dye, eosin Y, as spectroscopic probe in chemical and pharmaceutical analysis; a review, *Rev. Anal. Chem.*, 2018, **37**, 20170020.
4 G. O. Ogunlusi, O. D. Amos, O. F. Olatunji and A. A. Adenuga, Equilibrium, kinetic, and thermodynamic studies of the adsorption of anionic and cationic dyes from aqueous solution using agricultural waste biochar, *J. Iran. Chem. Soc.*, 2023, **20**, 817–830.
5 T. A. Bhutto, M. A. Jakhrani, A. A. Jamali, J. A. Buledi, R. D. Janwary, A. Hyder, K. H. Chachar and N. H. Kalwar, Strategic fabrication of PVP caped CuO hetero-catalyst for degradation of Eosin Y: a decontamination study, *J. Iran. Chem. Soc.*, 2023, **20**, 1225–1235.
6 Z. Chen, X. Li, Q. Xu, Z. Tao, F. Yao, X. Huang, Y. Wu, D. Wang, P. Jiang and Q. Yang, Three-dimensional network space Ag_3PO_4/NP-CQDs/rGH for enhanced organic pollutant photodegradation: Synergetic photocatalysis activity/stability and effect of real water quality parameters, *Chem. Eng. J.*, 2020, **390**, 124454.
7 A. Alexandra Sanchez, N. Mladenov and J. Wasswa, Fluorescent compounds retained by ultrafiltration membranes for water reuse, *J. Membr. Sci.*, 2020, **600**, 117867.
8 I. González-Mariño, J. B. Quintana, I. Rodríguez and R. Cela, Evaluation of the occurrence and biodegradation of parabens and halogenated by-products in wastewater by accurate-mass liquid chromatography-quadrupole-time-of-flight-mass spectrometry (LC-QTOF-MS), *Water Res.*, 2011, **45**, 6770–6780.
9 Y. Luo, W. Guo, H. H. Ngo, L. D. Nghiem, F. I. Hai, J. Zhang, S. Liang and X. C. Wang, A review on the occurrence of micropollutants in the aquatic environment and their fate and removal during wastewater treatment, *Sci. Total Environ.*, 2014, **473–474**, 619–641.
10 N. Sharma, R. Jha, S. Baghel and D. Sharma, Study on photocatalyst Zinc Oxide annealed at different temperatures for photodegradation of Eosin Y dye, *J. Alloys Compd.*, 2017, **695**, 270–279.
11 S. K. Yadav, S. R. Dhakate and B. Pratap Singh, Carbon nanotube incorporated eucalyptus derived activated carbon-based novel adsorbent for efficient removal of methylene blue and eosin yellow dyes, *Bioresour. Technol.*, 2022, **344**, 126231.
12 K. Yin, M.-G. Li, Y.-G. Chao, Y. Zhou, S.-J. Guo, F.-Z. Liu and H.-B. Li, Highly electronegative PtAu alloy for simultaneous hydrogen generation and ethanol upgrading, *Rare Met.*, 2023, **42**, 2949–2956.
13 Y. Zhang, Z. Zhang, H. Han, M. Zhang, H. Wang, H. Song and Y. Chen, Effective removal of organic dyes using the ultrasonic-assisted hydrothermal synthesis of NaP zeolite doping Cu or Fe in Fenton-like oxidation systems, *Sep. Purif. Technol.*, 2022, **299**, 121767.
14 S. Islam, I. A. Shaikh, N. Firdous, A. Ali and Y. Sadef, A new approach for the removal of unfixed dyes from reactive dyed cotton by Fenton oxidation, *J. Water Reuse Desalin.*, 2019, **9**, 133–141.
15 L. Wang, J. Li, Z. Wang, L. Zhao and Q. Jiang, Low-temperature hydrothermal synthesis of α-Fe/Fe_3O_4 nanocomposite for fast Congo red removal, *Dalton Trans.*, 2013, **42**, 2572–2579.
16 C. Xiao, J. Li and G. Zhang, Synthesis of stable burger-like α-Fe_2O_3 catalysts: Formation mechanism and excellent photo-Fenton catalytic performance, *J. Cleaner Prod.*, 2018, **180**, 550–559.
17 C. Xiao, X. Li, Q. Li, Y. Hu, J. Cheng and Y. Chen, Ni-doped FeC_2O_4 for efficient photo-Fenton simultaneous degradation of organic pollutants and reduction of Cr(VI): Accelerated Fe(III)/Fe(II) cycle, enhanced stability and mechanism insight, *J. Cleaner Prod.*, 2022, **340**, 130775.
18 Q. He, C. Xie, D. Gan and C. Xiao, The efficient degradation of organic pollutants in an aqueous environment under visible light irradiation by persulfate catalytically activated with kaolin-Fe_2O_3, *RSC Adv.*, 2020, **10**, 43–52.

19 C. Xiao, S. Li, F. Yi, B. Zhang, D. Chen, Y. Zhang, H. Chen and Y. Huang, Enhancement of photo-Fenton catalytic activity with the assistance of oxalic acid on the kaolin FeOOH system for the degradation of organic dyes, *RSC Adv.*, 2020, **10**, 18704–18714.
20 H. R. Rajabi, O. Khani, M. Shamsipur and V. Vatanpour, High-performance pure and Fe3+-ion doped ZnS quantum dots as green nanophotocatalysts for the removal of malachite green under UV-light irradiation, *J. Hazard. Mater.*, 2013, **250–251**, 370–378.
21 M. F. Lanjwani, M. Tuzen, M. Y. Khuhawar and T. A. Saleh, Trends in photocatalytic degradation of organic dye pollutants using nanoparticles: A review, *Inorg. Chem. Commun.*, 2024, **159**, 111613.
22 A. Bhattacharjee and M. Ahmaruzzaman, Facile synthesis of SnO_2 quantum dots and its photocatalytic activity in the degradation of eosin Y dye: A green approach, *Mater. Lett.*, 2015, **139**, 418–421.
23 G.-J. Lee and J. J. Wu, Recent developments in ZnS photocatalysts from synthesis to photocatalytic applications—A review, *Powder Technol.*, 2017, **318**, 8–22.
24 A. Nabiyan, J. B. Max, C. Neumann, M. Heiland, A. Turchanin, C. Streb and F. H. Schacher, Polyampholytic Graft Copolymers as Matrix for TiO_2/Eosin Y/$Mo_3S_{13}^{2-}$ Hybrid Materials and Light-Driven Catalysis, *Chem. – Eur. J*, 2021, **27**, 16924–16929.
25 X. Zheng, W. Fu, H. Peng and J. Wen, Preparation and characterization of CuxZn1-xS nanodisks for the efficient visible light photocatalytic activity, *J. Environ. Chem. Eng.*, 2018, **6**, 9–18.
26 X.-H. Guan, P. Qu, X. Guan and G.-S. Wang, Hydrothermal synthesis of hierarchical CuS/ZnS nanocomposites and their photocatalytic and microwave absorption properties, *RSC Adv.*, 2014, **4**, 15579–15585.
27 A. J. Howarth, T. C. Wang, S. S. Al-Juaid, S. G. Aziz, J. T. Hupp and O. K. Farha, Efficient extraction of sulfate from water using a Zr-metal–organic framework, *Dalton Trans.*, 2016, **45**, 93–97.
28 J. Patel, K. R. Singh, A. K. Singh, J. Singh and A. K. Singh, Multifunctional Cu:ZnS quantum dots for degradation of Amoxicillin and Dye Sulphon Fast Black-F and efficient determination of urea for assessing environmental aspects, *Environ. Res.*, 2023, **235**, 116674.
29 Y. Wang, Y. Long, Z. Yang and D. Zhang, A novel ion-exchange strategy for the fabrication of high strong BiOI/BiOBr heterostructure film coated metal wire mesh with tunable visible-light-driven photocatalytic reactivity, *J. Hazard. Mater.*, 2018, **351**, 11–19.
30 H.-J. Chen, Y.-L. Yang, M. Hong, J.-G. Chen, G.-Q. Suo, X.-J. Hou, L. Feng and Z.-G. Chen, Separable and recyclable meso-carbon@TiO_2/carbon fiber composites for visible-light photocatalysis and photoelectrocatalysis, *Sustainable Mater. Technol.*, 2019, **21**, e00105.
31 Y. Yang, H. Chen, X. Zou, X.-L. Shi, W.-D. Liu, L. Feng, G. Suo, X. Hou, X. Ye, L. Zhang, C. Sun, H. Li, C. Wang and Z.-G. Chen, Flexible Carbon-Fiber/Semimetal Bi Nanosheet Arrays as Separable and Recyclable Plasmonic Photocatalysts and Photoelectrocatalysts, *ACS Appl. Mater. Interfaces*, 2020, **12**, 24845–24854.
32 E. M. Sitinjak, I. Masmur, N. V. M. D. Marbun, P. E. Hutajulu, G. Gultom and Y. Sitanggang, Direct Z-scheme of n-type CuS/p-type ZnS@electrospun PVP nanofiber for the highly efficient catalytic reduction of 4-nitrophenol and mixed dyes, *RSC Adv.*, 2022, **12**, 16165–16173.
33 U. T. D. Thuy, I. Borisova, O. Stoilova, I. Rashkov and N. Q. Liem, Electrospun CuS/ZnS–PAN Hybrids as Efficient Visible-Light Photocatalysts, *Catal. Lett.*, 2018, **148**, 2756–2764.
34 P. Das, K. Tantubay, R. Ghosh, S. Dam and M. Baskey, Transformation of CuS/ZnS nanomaterials to an efficient visible light photocatalyst by 'photosensitizer' graphene and the potential antimicrobial activities of the nanocomposites, *Environ. Sci. Pollut. Res.*, 2021, **28**, 49125–49138.
35 J. Esmaili-Hafshejani and A. Nezamzadeh-Ejhieh, Increased photocatalytic activity of Zn(II)/Cu(II) oxides and sulfides by coupling and supporting them onto clinoptilolite nanoparticles in the degradation of benzophenone aqueous solution, *J. Hazard. Mater.*, 2016, **316**, 194–203.
36 W. Xie, C. Guo, Y. Zhao, L. Chen, B. Liao and S. Zhang, Development of Ti/Ti-DLC multilayers on magnesium alloys-Part 2: Corrosion and wear resistance, *Surf. Coat. Technol.*, 2024, **477**, 130332.
37 K. Zhao, Y. Ge, J. Wang, Y. Liu, Y. Wu, X. Yu, S. Zhuang, H. Cao, Y. Zhao, X. Yang and X. Gu, Silk fibroin-based hydrogels with low hysteresis, self-adhesion, and tunable ionic conductivity for wearable devices, *Int. J. Biol. Macromol.*, 2025, **306**, 141597.
38 Y. Huang, X. Wu, T. Tian, Z. Zhu, H. Lin and C. Yang, Target-responsive DNAzyme hydrogel for portable colorimetric detection of lanthanide(III) ions, *Sci. China: Chem.*, 2017, **60**, 293–298.
39 J. Wang, Y. Wu, K. Zhao, G. Liu, R. Wang, Y. Zhao, Y. Liu, Y. Ge, X. Jiang and X. Gu, Mechanically Robust, Time-Programmable, Janus Hydrogel Actuator, and the Insights into Its Driving Principles, *ACS Appl. Polym. Mater.*, 2025, **7**, 3670–3685.
40 W. Liao, M. Zhao, H. Rong, P. Jiang, Q. Liao, C. Zhang and Y. Chen, Photocatalyst immobilized by hydrogel, efficient degradation and self regeneration: A review, *Mater. Sci. Semicond. Process.*, 2022, **150**, 106929.
41 J. Yang, D. Chen, Y. Zhu, Y. Zhang and Y. Zhu, 3D-3D porous Bi_2WO_6/graphene hydrogel composite with excellent synergistic effect of adsorption-enrichment and photocatalytic degradation, *Appl. Catal., B*, 2017, **205**, 228–237.
42 Y. Qin, H. Zhao, Q. Wang, X. Zhang and Y. Li, Well controlled reduction, N-doping and cross-linking of graphene hydrogel: As good template for photocatalytic reaction, *Appl. Surf. Sci.*, 2020, **528**, 146945.
43 Y. Qin, J. Luo, Q. An, Z. Xiao, J. Hao, Y. Tong and S. Zhai, Three-dimensional Co-N/SBA-15/alginate hydrogels with excellent recovery and recyclability for activating peroxymonosulfate to

degrade ciprofloxacin, *Micropor. Mesopor. Mater.*, 2021, **323**, 111259.

44 W. Gao, H. Kang, M. Zhong, L. Han, X. Guo, B. Su and Z. Lei, Chitosan-Promoted TiO_2-Loaded Double-Network Hydrogels for Dye Removal and Wearable Sensors, *Biomacromolecules*, 2024, **25**, 8016–8025.

45 A. K. Mohamed and M. E. Mahmoud, Encapsulation of starch hydrogel and doping nanomagnetite onto metal-organic frameworks for efficient removal of fluvastatin antibiotic from water, *Carbohydr. Polym.*, 2020, **245**, 116438.

46 J. Li, X. Yu, Y. Zhu, X. Fu and Y. Zhang, 3D-2D-3D BiOI/porous g-C3N4/graphene hydrogel composite photocatalyst with synergy of adsorption-photocatalysis in static and flow systems, *J. Alloys Compd.*, 2021, **850**, 156778.

47 M. Farooq, J. Ihsan, R. M. K. Mohamed, M. A. Khan, T. U. Rehman, H. Ullah, M. Ghani, S. Saeed and M. Siddiq, Highly biocompatible formulations based on Arabic gum Nano composite hydrogels: Fabrication, characterization, and biological investigation, *Int. J. Biol. Macromol.*, 2022, **209**, 59–69.

48 H. Du, A. Zhang, Q. Zhang, Y. Sun, H. Zhu, H. Wang, Z. Tan, X. Zhang and G. Chen, Fabrication of recoverable Bi_2O_2S/Bi_5O_7I/ZA hydrogel beads for enhanced photocatalytic Hg0 removal in the presence of H_2O_2, *Sep. Purif. Technol.*, 2025, **359**, 130597.

49 J. Wang, X. Li, Q. Cheng, F. Lv, C. Chang and L. Zhang, Construction of β-FeOOH@tunicate cellulose nanocomposite hydrogels and their highly efficient photocatalytic properties, *Carbohydr. Polym.*, 2020, **229**, 115470.

50 Y. Du, H. Che, P. Wang, J. Chen and Y. Ao, Highly efficient removal of organic contaminant with wide concentration range by a novel self-cleaning hydrogel: Mechanism, degradation pathway and DFT calculation, *J. Hazard. Mater.*, 2022, **440**, 129738.

51 H. Zhu, Z. Li and J. Yang, A novel composite hydrogel for adsorption and photocatalytic degradation of bisphenol A by visible light irradiation, *Chem. Eng. J.*, 2018, **334**, 1679–1690.

52 Y. Işikver, Removal of some cationic dyes from aqueous solution by acrylamide- or 2-hydroxyethyl methacrylate-based copolymeric hydrogels, *Fibers Polym.*, 2017, **18**, 2070–2078.

53 O. Ejeromedoghene, X. Zuo, O. Oderinde, F. Yao, S. Adewuyi and G. Fu, Photochromic Behavior of Inorganic Superporous Hydrogels Fabricated from Different Reacting Systems of Polymeric Deep Eutectic Solvents, *J. Mol. Struct.*, 2023, **1271**, 134101.

54 X.-H. Guan, P. Qu, X. Guan and G.-S. Wang, Hydrothermal synthesis of hierarchical CuS/ZnS nanocomposites and their photocatalytic and microwave absorption properties, *RSC Adv.*, 2014, **4**, 15579–15585.

55 Z. Qing, L. Wang, X. Liu, Z. Song, F. Qian and Y. Song, Simply synthesized sodium alginate/zirconium hydrogel as adsorbent for phosphate adsorption from aqueous solution: Performance and mechanisms, *Chemosphere*, 2022, **291**, 133103.

56 X. Zheng, W. Fu, H. Peng and J. Wen, Preparation and characterization of CuxZn1-xS nanodisks for the efficient visible light photocatalytic activity, *J. Environ. Chem. Eng.*, 2018, **6**, 9–18.

57 R. Liu, Z. Ji, J. Wang and J. Zhang, Solvothermal fabrication of TiO2/sepiolite composite gel with exposed {001} and {101} facets and its enhanced photocatalytic activity, *Appl. Surf. Sci.*, 2018, **441**, 29–39.

58 S. J. Allen, Q. Gan, R. Matthews and P. A. Johnson, Kinetic modeling of the adsorption of basic dyes by kudzu, *J. Colloid Interface Sci.*, 2005, **286**, 101–109.

59 V. K. Gupta and A. Rastogi, Biosorption of lead from aqueous solutions by green algae Spirogyra species: Kinetics and equilibrium studies, *J. Hazard. Mater.*, 2008, **152**, 407–414.

60 G. Yang, H. Han, C. Du, Z. Luo and Y. Wang, Facile synthesis of melamine-based porous polymer networks and their application for removal of aqueous mercury ions, *Polymer*, 2010, **51**, 6193–6202.

61 Y. Habba, M. Capochichi-Gnambodoe and Y. Leprince-Wang, Enhanced Photocatalytic Activity of Iron-Doped ZnO Nanowires for Water Purification, *Appl. Sci.*, 2017, **7**, 1185.

62 S. M. Taheri Otaqsara, Red luminescence of spherical $Cu_xZn_{1-x}S$ semiconductor nanoparticles using 2-mercaptoethanol as capping agent, *Mater. Sci. Semicond. Process.*, 2013, **16**, 963–970.

63 X. Zheng, W. Fu, H. Peng and J. Wen, Preparation and characterization of $Cu_xZn_{1-x}S$ nanodisks for the efficient visible light photocatalytic activity, *J. Environ. Chem. Eng.*, 2018, **6**, 9–18.

64 M. Bhushan and R. Jha, Surface activity correlations of mesoporous 3-D hierarchical ZnS nanostructures for enhanced photo and electro catalytic performance, *Appl. Surf. Sci.*, 2020, **528**, 146988.

